

Article

Modulation Format Identification Based on Multi-Dimensional Amplitude Features for Elastic Optical Networks

Ming Hao ^{1,2,*}, Wei He ¹, Xuedong Jiang ¹ , Shuai Liang ¹, Wei Jin ³ , Lin Chen ⁴  and Jianming Tang ³

- ¹ School of Automation and Information Engineering, Sichuan University of Science and Engineering, Yibin 644000, China
- ² Artificial Intelligence Key Laboratory of Sichuan Province, Sichuan University of Science and Engineering, Yibin 644000, China
- ³ The DSP Centre of Excellence, School of Computer Science and Electronic Engineering, Bangor University, Bangor LL57 1UT, UK
- ⁴ College of Electronics and Information Engineering, Shanghai University of Electric Power, Shanghai 200090, China
- * Correspondence: haoming@suse.edu.cn

Abstract: A modulation format identification (MFI) scheme based on multi-dimensional amplitude features is proposed for elastic optical networks. According to the multi-dimensional amplitude features, incoming polarization division multiplexed (PDM) signals can be identified as QPSK, 8QAM, 16QAM, 32QAM, 64QAM and 128QAM signals using the k-nearest neighbors (KNNs) algorithm in the digital coherent receivers. The proposed scheme does not require any prior training or optical signal-to-noise ratio (OSNR) information. The performance of the proposed MFI scheme is verified based on numerical simulations with 28GBaud PDM-QPSK/-8QAM/-16QAM/-32QAM/-64QAM/-128QAM signals. The results show that the proposed scheme can achieve 100% of the correct MFI rate for all six modulation formats when the OSNR values are greater than their thresholds corresponding to the 20% forward error correction (FEC) related to a BER of 2.4×10^{-2} . Meanwhile, the effects of residual chromatic dispersion, polarization mode dispersion and fiber nonlinearities on the proposed scheme are also explored. Finally, the computational complexity of the proposed scheme is analyzed, which is compared with relevant MFI schemes. The work indicates that the proposed technique could be regarded as a good candidate for identifying modulation formats up to 128QAM.



Citation: Hao, M.; He, W.; Jiang, X.; Liang, S.; Jin, W.; Chen, L.; Tang, J. Modulation Format Identification Based on Multi-Dimensional Amplitude Features for Elastic Optical Networks. *Photonics* **2024**, *11*, 390. <https://doi.org/10.3390/photonics11050390>

Received: 27 March 2024
Revised: 12 April 2024
Accepted: 19 April 2024
Published: 23 April 2024



Copyright: © 2024 by the authors. Licensee MDPI, Basel, Switzerland. This article is an open access article distributed under the terms and conditions of the Creative Commons Attribution (CC BY) license (<https://creativecommons.org/licenses/by/4.0/>).

Keywords: modulation format identification; multi-dimensional amplitude feature; k-nearest neighbors algorithm; coherent optical communications

1. Introduction

The adaptation of high-order modulation formats is regarded as one of the most effective schemes to improve both the spectral efficiency and the existing optical fiber infrastructure utilization efficiency [1]. However, for a given optical transmission system, the highest achievable order of the modulation format is limited by its anti-noise performance and tolerance to linear and/or nonlinear transmission system impairments. Meanwhile, the optical network is required to meet heterogeneous and dynamic demands for supporting diverse data services, such as 5G, cloud computing, big data and the internet of things by optimizing the allocation of the bandwidth and modulation format. As a direct result, the optical network is evolving from fixed network architectures to flexible and elastic ones [2,3]. In elastic optical networks (EONs), according to different channel characteristics and various data services, the involved transceivers can dynamically adjust the modulation formats utilized for encoding the optical signals, which raises new demands on digital coherent receivers. Therefore, the MFI module embedded in a digital coherent receiver, which can identify the modulation format of incoming signals on-the-fly, is of great importance [4]. MFI provides a foundation for optimizing the performance of subsequent

modulation format-dependent algorithms in the digital signal processing (DSP) chain; as such, MFI is a critical technology to ensure the flexibility and reliability of the EON.

The previously reported MFI schemes for EON can be classified into data-aided and non-data-aided schemes [5–7]. Since additional pilot information is introduced in the transmitter, the computational complexity of the data-aided schemes [8–10] is thus low with an additional cost of a reduced spectral efficiency. On the other hand, without any special coding, the non-data-aided schemes can identify modulation formats based on the extracted features of the received signals. Non-data-aided schemes can be further roughly divided into schemes based on Stokes space and schemes based on the signal equalized by the constant modulus algorithm (CMA). Schemes based on Stokes space [11–22] are not sensitive to carrier phase noise, frequency offset or polarization mixing. However, it is difficult for these schemes to identify high-order modulation formats, which have a large number of clusters. On the flip side, the schemes based on CMA-equalized signals [23–32] do not require any space mapping, and CMA can partially compensate for residual chromatic dispersion (CD) and polarization mode dispersion (PMD) [33,34]. However, all of these schemes mentioned above are only suitable for identifying modulation formats up to 64QAM.

Generally speaking, the modulation format identification difficulty increases significantly upon increasing the modulation format order. To address this problem, an MFI scheme based on signal constellation diagrams and support vector machine (SVM) has been proposed in [35], which identifies modulation formats up to 256QAM at the cost of computational complexity in the feature-extraction stage. The authors in [36] have proposed an MFI scheme that utilizes a peak-density clustering algorithm to identify constellation diagrams of modulation formats up to 128QAM for adaptive optical OFDM systems. Zhang et al. [37] have demonstrated a simultaneous MFI and OSNR monitoring scheme for QPSK, 8QAM, 16QAM, 32QAM, 64QAM and 128QAM signals based on multi-task model-agnostic meta-learning. An MFI scheme based on amplitude variance and OSNR information of the received signals has been proposed in [38], which can identify modulation formats up to 2048QAM. However, the acceptable OSNR measurement error for this scheme is only ± 0.2 dB.

In this paper, an MFI scheme based on multi-dimensional amplitude features is proposed for practical implementations in autonomous digital coherent receivers. In the proposed MFI scheme, after having performed power normalization, the numbers of CMA-equalized symbols in six specific amplitude ranges are calculated, based on which the six-dimensional feature of the incoming signals is constructed for the identification of different modulation formats. Since there are different amplitude levels for QPSK, 8QAM, 16QAM, 32QAM, 64QAM and 128QAM, the specific amplitude features of different modulation formats exhibit obviously different distributions in the six-dimensional space. Therefore, the multi-dimensional amplitude feature of the six modulation formats can be subsequently identified by KNN. The performance of the proposed MFI scheme is verified based on numerical simulations with 28GBaud PDM-QPSK/-8QAM/-16QAM/-32QAM/-64QAM/-128QAM signals. The results show that the proposed scheme can achieve 100% of the correct MFI rate for all of the six modulation formats when their corresponding OSNR values are higher than their theoretical 20% FEC limit. The simulation results also demonstrate that the proposed scheme is robust against both linear and nonlinear impairments. Finally, the computational complexity of the proposed scheme is analyzed. Our results indicate that the proposed technique can be regarded as a good candidate for identifying modulation formats up to 128QAM.

2. Operating Principle

As depicted in Figure 1, the DSP chain for a digital coherent receiver consists of modulation-format-independent algorithms and modulation-format-dependent algorithms. The proposed MFI scheme is located between the modulation-format-independent algorithms and the modulation-format-dependent algorithms. Based on modulation-format-

independent algorithms, the CD impairments and timing-jitters are compensated for, respectively, and the polarization demultiplexing is also preliminary achieved. Subsequently, the proposed MFI scheme is applied based on CMA-equalized signals and provides the information to the modulation-format-dependent algorithms (multi modulus algorithm (MMA), frequency offset compensation and carrier phase recovery) and symbol de-mapping.

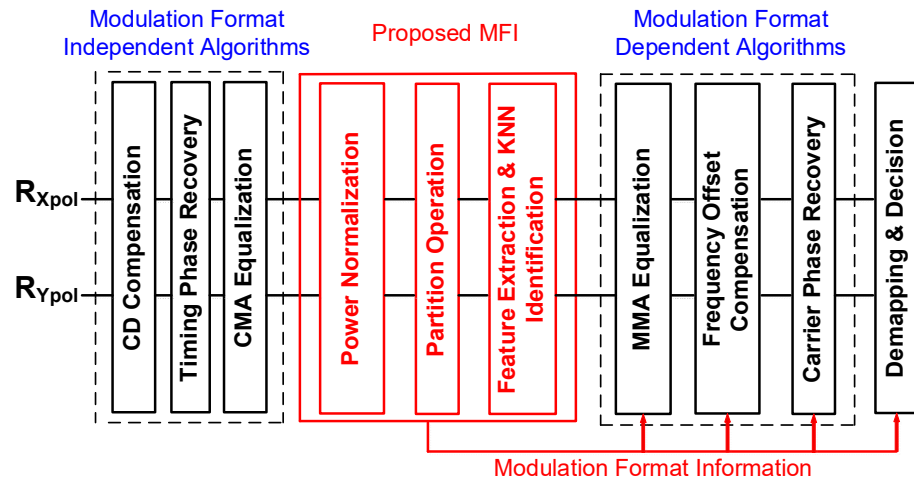


Figure 1. The DSP architecture with the proposed MFI scheme for digital coherent receivers.

As shown in Figure 1, the proposed MFI scheme comprises three steps; firstly, power normalization of the CMA equalized signals is performed. Secondly, the amplitude histogram is obtained, which is then divided into six specific amplitude ranges. Finally, the numbers of symbols in the six specific amplitude ranges are calculated, based on which the six-dimensional feature of the incoming signals is constructed. The multi-dimensional amplitude feature of different modulation formats is subsequently identified by KNN.

The six modulation formats (QPSK, 8QAM, 16QAM, 32QAM, 64QAM and 128QAM) have different amplitude levels and are theoretically easy to identify. However, under the influence of the channel noise, residual CD, PMD and fiber nonlinearities, the amplitude features of the received signals in practical transmission systems are difficult to recognize, especially for high-order modulation formats. The amplitude histograms of these six modulation formats are illustrated in Figure 2, where the OSNR values for the PDM-QPSK/-8QAM/-16QAM/-32QAM/-64QAM/-128QAM signals are 26 dB, 31 dB, 33 dB, 36 dB, 38 dB and 40 dB, respectively. The amplitude histograms shown in Figure 2 are obtained utilizing 8000 symbols, which are grouped into 40 bins between the maximum and minimum amplitude values of the CMA-equalized signals. As shown in Figure 2, even for high OSNR cases, the different amplitude levels of high-order modulation formats cannot be easily distinguishable. Therefore, relying solely on the global feature of the amplitude histogram cannot identify signal modulation formats higher than for 128QAM.

To address such a challenge, the scheme proposed in this paper adopts a more efficient local feature extraction approach. As illustrated in Figure 2, the numbers (N_1, N_2, N_3, N_4, N_5 and N_6) of the CMA-equalized symbols in six specific amplitude ranges ($A_1 \sim B_1, A_2 \sim B_2, A_3 \sim B_3, A_4 \sim B_4, A_5 \sim B_5$ and $A_6 \sim B_6$) are utilized to construct six-dimensional features of the incoming signals. As shown in Figure 2a, due to the constant amplitude of QPSK, as noise or other transmission impairments gives rise to few symbols deviated from the constant amplitude, the number of symbols within the range from A_1 to B_1 is thus very small. Therefore, N_1 within the range of $A_1 \sim B_1$ can be employed to separate QPSK from the other five modulation formats. For the same reason, as shown in Figure 2b, N_2 for the range of ($A_2 \sim B_2$) (the number of symbols distributed in the second half of the first amplitude peak of 8QAM) can be used as a feature for identifying 8QAM. Similarly, N_3 and N_4 , representing the numbers of the symbols distributed in the first half of the first

amplitude peak of 16QAM, ($A_3 \sim B_3$), and the first half of the first amplitude peak of 32QAM, ($A_4 \sim B_4$), can be employed as distinct features for identifying 16QAM and 32QAM, respectively. Although there are nine amplitude levels for 64QAM, its corresponding amplitude histogram does not, however, clearly illustrate nine distinguishable levels in the presence of noise. Since the associated probability for the sixth amplitude level of 64QAM is highest [3], N_5 , representing the number of symbols within the range of ($A_5 \sim B_5$), can thus be calculated to extract the feature for 64QAM. N_1, N_2, N_3, N_4 and N_5 mainly represent the features located in the front and middle of the relevant histograms, whilst N_6 for 128QAM extracts the feature located in the last part of the histogram. 128QAM exhibits different distributions within the range of ($A_6 \sim B_6$). The ranges $A_1 \sim B_1, A_2 \sim B_2, A_3 \sim B_3, A_4 \sim B_4, A_5 \sim B_5$ and $A_6 \sim B_6$ are 1~16, 14~22, 4~12, 1~8, 25~28 and 34~40, respectively. It should be noted that the identification performance is dependent on the effectiveness and irreplaceability of features rather than dimensions of the feature. Excessive features would lead to confusion among different modulation formats in the multi-dimensional space, and thus, only six dimensional features are selected.

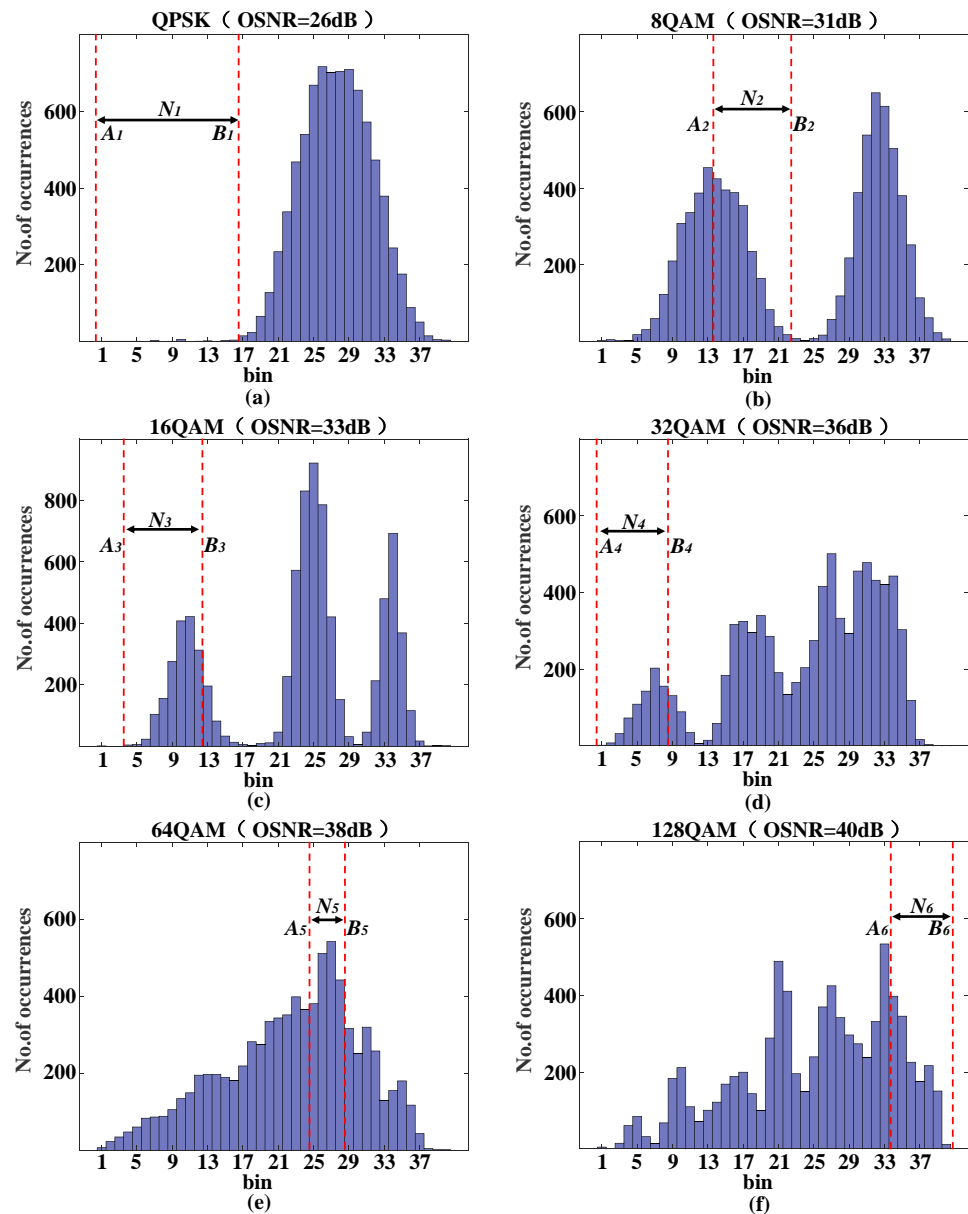


Figure 2. The amplitude histograms of (a) QPSK, (b) 8QAM, (c) 16QAM, (d) 32QAM, (e) 64QAM, (f) 128QAM and the corresponding partition operation.

Due to the noise effect, even the features of the same modulation format may appear to be different for different OSNR conditions, but the distribution of the different modulation formats in the six-dimensional space is still sharply distinguishable. In order to verify the above statement, Figure 3 is plotted, where the features in a three-dimensional space are shown by using three of the six features as coordinates (N_1, N_2, N_4 for Figure 3a–c, N_1, N_5, N_6 for Figure 3d and N_1, N_3, N_4 for Figure 3e,f). The distribution of the six modulation formats in the three-dimensional space based on N_1, N_2 and N_4 is illustrated in Figure 3a. Two different views of Figure 3a from two different angles are given for (QPSK, 8QAM, 16QAM) in Figure 3b and (32QAM, 64QAM, 128QAM) in Figure 3c. From Figure 3a,b, it can be clearly seen that QPSK and 8QAM can be easily distinguished from the other four modulation formats. Meanwhile, 32QAM, 64QAM and 128QAM are also distinguishable among each other. As shown in Figure 3a, 16QAM is not distinguishable from 32QAM, 64QAM and 128QAM in the three-dimensional space (N_1, N_2 and N_4). However, as shown in Figure 3d–f, 16QAM can be distinguished easily from 32QAM, 64QAM and 128QAM based on the other three features (N_1, N_5 and N_6 for separating 32QAM, and N_1, N_3 and N_4 for separating 64QAM or 128QAM), respectively. The above analysis indicates that when the six-dimensional features are regarded as a whole, the six modulation formats can be identified.

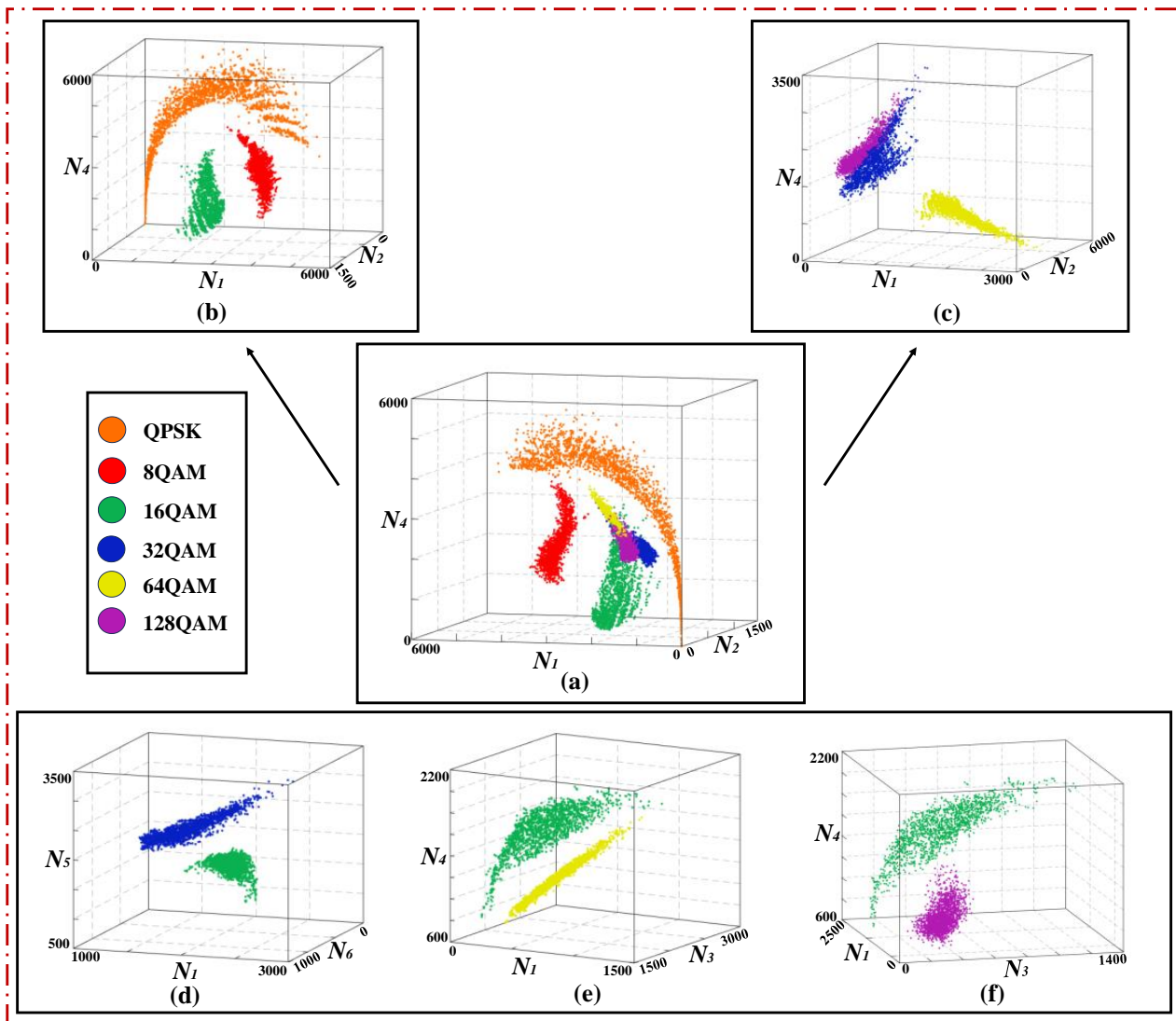


Figure 3. The three-dimensional space composed of features (a–c) N_1, N_2 and N_4 , (d) N_1, N_5 and N_6 and (e,f) N_1, N_3 and N_4 for different modulation formats.

KNN is an effective supervised learning algorithm commonly used in classification problems. As shown in Figure 3, the modulation format of an incoming signal can be easily determined by nearby training samples in the six-dimensional space. Compared with another classification algorithm SVM, which makes decisions based on hyperplanes, KNN is more suitable for identifying the extracted features. Therefore, as depicted in Figure 4, KNN is employed to recognize the six-dimensional features (N_1, N_2, N_3, N_4, N_5 and N_6). The Euclidean distance d between a test sample and each training sample in the six dimensional space is calculated as

$$d = \sqrt{\sum_{j=1}^6 (x_{1j} - x_{2j})^2} \tag{1}$$

where x_{1j} denotes the j -th feature of the test sample, and x_{2j} represents the j -th feature of the training sample. According to the size of the k value, the KNN finds k training samples in the training dataset that are closest to the test sample, and then, for a randomly given category i , the number of occurrences of the category in the k nearest training samples is known. Finally, as shown in Equation (2), the category of the test sample is determined based on the category with the most occurrences among the k nearest training samples.

$$i^* = \operatorname{argmax}_i V(i; x_{test}) \tag{2}$$

where V is the occurrences among the k nearest training samples for category i , and i^* is the determined category for the test sample. Since the input of KNN is only six-dimensional, the extracted local amplitude feature not only represents the characteristic of modulation format, but also significantly reduces the complexity of KNN compared to the global feature.

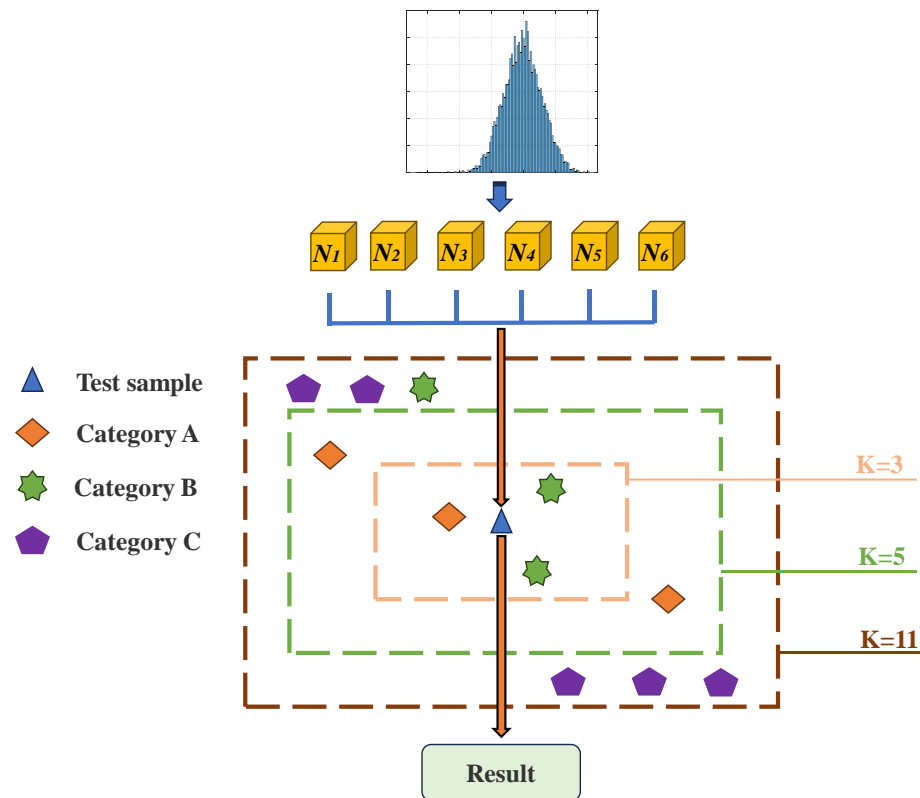


Figure 4. Schematic diagram of identification by KNN.

3. Results and Analysis

To verify the proposed scheme, a series of numerical simulations is conducted based on *VPI Transmission Maker 9.8*. The simulation setup of a PDM coherent optical transmission system is illustrated in Figure 5. In all of the simulations, external cavity laser (ECL) is operated with 100 kHz linewidths. Six modulation format (QPSK, 8QAM, 16QAM, 32QAM, 64QAM and 128QAM)-encoded optical signals are generated by driving the I/Q modulator with a binary 28Gbaud electrical signal. The transmission links comprise back-to-back (BTB) and long-distance fiber transmissions. The OSNR value of the BTB case is adjusted by the Set OSNR module. The OSNR ranges of the PDM-QPSK/-8QAM/-16QAM/-32QAM/-64QAM/-128QAM-encoded signals are 5~24 dB, 10~29 dB, 12~31 dB, 16~35 dB, 17~36 dB and 23~42 dB, respectively. The long-distance transmission link is composed of $M \times 80$ km ($M = 25$ for QPSK, $M = 20$ for 8QAM, $M = 13$ for 16QAM, $M = 5$ for 32QAM, $M = 2$ for 64QAM, $M = 1$ for 128QAM) spans of single-mode fibers (SMFs) that have a dispersion parameter of $D = 16$ ps/nm/km, a PMD parameter of $D_{PMD} = 0.1$ ps/km^{1/2}, an attenuation of $\alpha = 0.2$ dB/km and a nonlinear coefficient of $\gamma = 1.267$ km⁻¹W⁻¹. The fiber loss of each span is completely compensated for per span using an erbium-doped fiber amplifier (EDFA) with a noise figure of 5 dB. At the receiving end, the incoming signals and the local oscillator (LO) are combined at a polarization diversity hybrid, and then, the photo is detected by a balanced photo-detector. Then, the digital signals that have been sampled by an analog to digital converter (ADC) are processed by an off-line DSP module. A training set is constructed by using eighty samples for each OSNR value and each modulation format in the BTB case, and the training set is then applied for both BTB and long-distance testing. Twenty samples are applied to validate a correct MFI rate for each OSNR value in the BTB case or for each launch power in the long-distance transmission case.

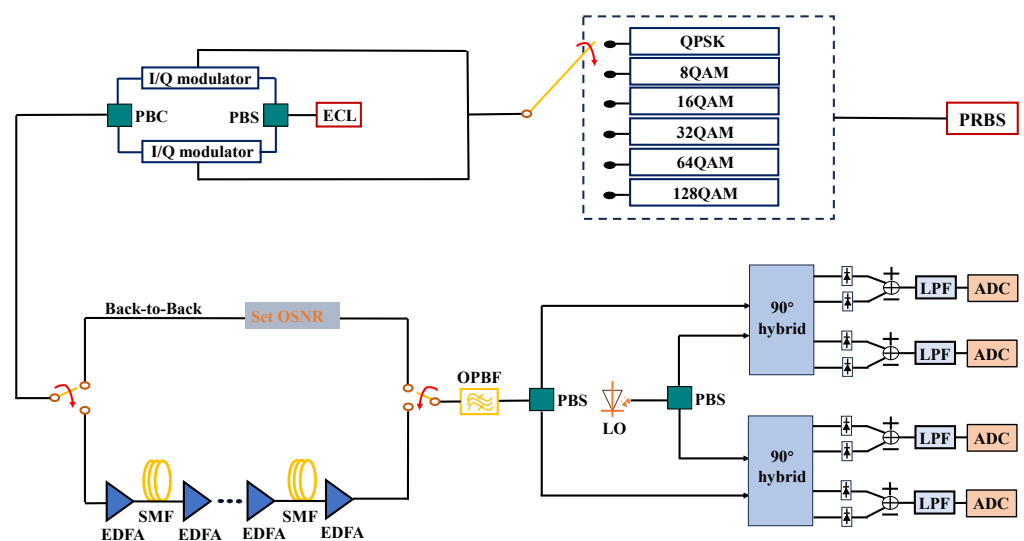


Figure 5. The simulation setup of the PDM coherent optical transmission system. PBS: polarization beam splitter; PBC: polarization beam combiner; LPE: low-pass filter.

The minimum required number of symbols determines the response-speed and computational complexity of the MFI algorithm [26]; on the other hand, too few symbols would result in a fuzzy feature, especially for high-order modulation formats. The minimum required OSNR values for the six modulation formats as a function of the number of symbols are shown in Figure 6a,b, and the step sizes are 1000 and 250, respectively. If the number of symbols is less than 7000, for most of these modulation formats, the minimum required OSNR values to achieve a 100% correct MFI rate increase accordingly. On the other hand, 128QAM requires more symbols to accurately extract the feature. In order to find the optimal number of symbols, the step size of the symbol number is decreased to 250 in Figure 6b. Although the minimum required OSNR value for 128QAM is optimal

when the number of symbols is 7500, the minimum required OSNR values for 8QAM, 16QAM, 32QAM and 64QAM are, however, greater than these for the 8000 symbols case. Considering the tradeoff between all the six modulation formats, the required numbers of symbols for the six modulation formats are thus fixed at 8000.

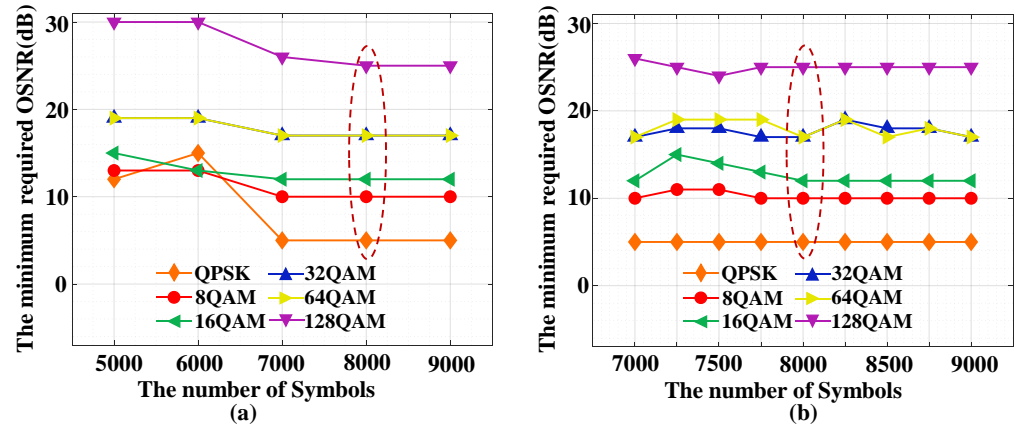


Figure 6. Minimum required OSNR values with different numbers of symbols for six modulation formats. The symbol number range for (a) is 5000~9000 with a 1000 step size and (b) is 7000~9000 with a 250 step size.

As analyzed in Section 2, the KNN determines the modulation format of an incoming signal based on the categories of the k nearest training samples. The value of k is an important parameter and determines the identification performance of KNN. Similar to the process used in Figure 6, an optimal k value should also be identified with the minimum required OSNR value. The simulated results are illustrated in Figure 7. When the value of k increases from 1 to 9, the minimum required OSNR values for QPSK, 8QAM and 64QAM remain unchanged, while the minimum required OSNR values for 16QAM and 32QAM increase slightly. It can also be clearly seen in Figure 7 that the optimal k value for 128QAM is 3. Therefore, for all of the considered modulation formats, the k value is taken to be 3.

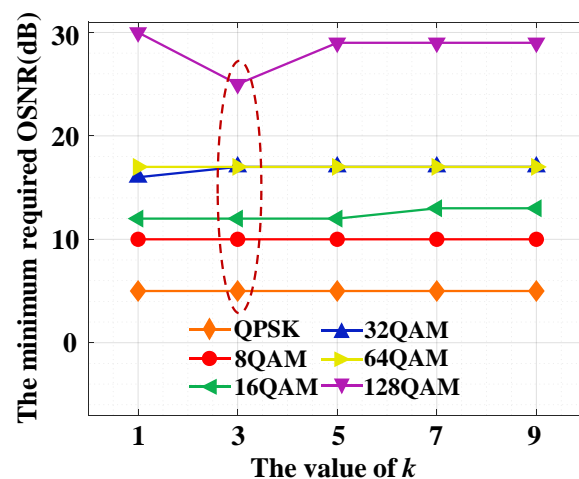


Figure 7. The minimum required OSNR values with different k values for six modulation formats.

To evaluate the identification performance of the proposed scheme, the correct MFI rate for each individual modulation format as a function of OSNR is shown in Figure 8. The vertical dash lines are the OSNR thresholds corresponding to the 20% FEC related to BERs of 2.4×10^{-2} . For QPSK, 8QAM, 16QAM, 32QAM and 64QAM, the proposed MFI scheme can achieve 100% of the correct MFI rate even if the OSNR value is much less than the corresponding theoretical 20% FEC limit. Since 128QAM is the highest order of the

six modulation formats, the minimum required OSNR for 128QAM is much higher than the other five modulation formats. Figure 8 indicates that the proposed MFI scheme can achieve 100% of the correct MFI rate for all six modulation formats when the OSNR values are greater than their corresponding thresholds related to the 20% FEC.

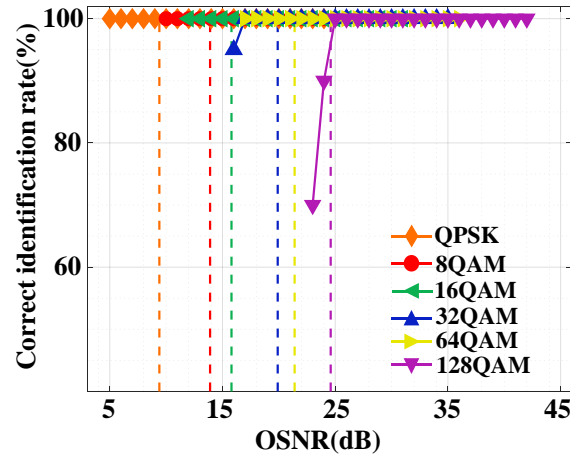


Figure 8. The correct MFI rate for the six modulation formats under different OSNR values.

In order to evaluate the effect of the residual CD on the MFI performance, numerical simulations have also been conducted under conditions of the OSNR values of QPSK, 8QAM, 16QAM, 32QAM, 64QAM and 128QAM being set at 12 dB, 17 dB, 19 dB, 22 dB, 24 dB and 28 dB, respectively. In addition, the range of the residual CD for QPSK, 8QAM, 16QAM and 32QAM signals is -1920 ps/nm~ 1920 ps/nm, while the ranges of the residual CD for 64QAM and 128QAM signals are -720 ps/nm~ 720 ps/nm and -360 ps/nm~ 360 ps/nm, respectively. The step sizes for the six modulation formats are both 120 ps/nm. As illustrated in Figure 9, the proposed MFI scheme can tolerate wide ranges of residual CD, i.e., -1920 ps/nm~ 1920 ps/nm for QPSK signals, -1560 ps/nm~ 1680 ps/nm for 8QAM signals and -1680 ps/nm~ 1440 ps/nm for 32QAM signals. The identification accuracy of 16QAM is still maintained at $>95\%$ over a wide residual CD range, while the tolerance with respect to the residual CD for 16QAM is only -480 ps/nm~ 720 ps/nm. Because of the existence of more amplitude levels for 64QAM and 128QAM, the sensitivity of the extracted features against residual CD is much greater than low-order modulation formats, and thus, the tolerances with respect to residual CD for 64QAM and 128QAM are much lower (-240 ps/nm~ 360 ps/nm for 64QAM, and -240 ps/nm~ 240 ps/nm for 128QAM).

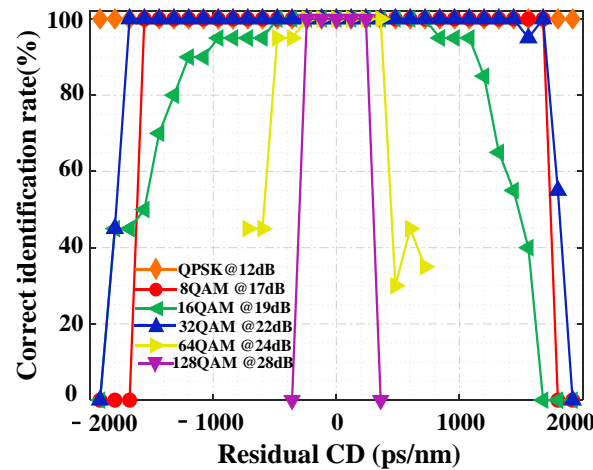


Figure 9. The tolerance with respect to the residual CD for the six modulation formats.

Simulations have also been undertaken to evaluate the effect of PMD on the MFI performance, and the simulated results are shown in Figure 10, in simulating which the range of differential-group delay (DGD) for QPSK, 8QAM, 16QAM and 32QAM signals is taken from 0 ps to 34 ps with a step size of 2 ps, while the range of DGD for 64QAM signals is taken from 0 ps to 22 ps with a step size of 2 ps. As shown in Figure 10a, the proposed scheme is able to achieve 100% of the correct MFI rate for the QPSK, 8QAM, 16QAM, 32QAM and 64QAM signals even when the DGDs are 34 ps, 32 ps, 16 ps, 20 ps and 10 ps, respectively. Compared to the aforementioned modulation formats, since 128QAM's DGD tolerance is significantly decreased, the range of DGD for 128QAM signals is from 0 ps to 2.4 ps with a step size of 0.2 ps. The tolerable DGD range for 128QAM signals is 1.6 ps, which is much lower than the other five modulation formats.

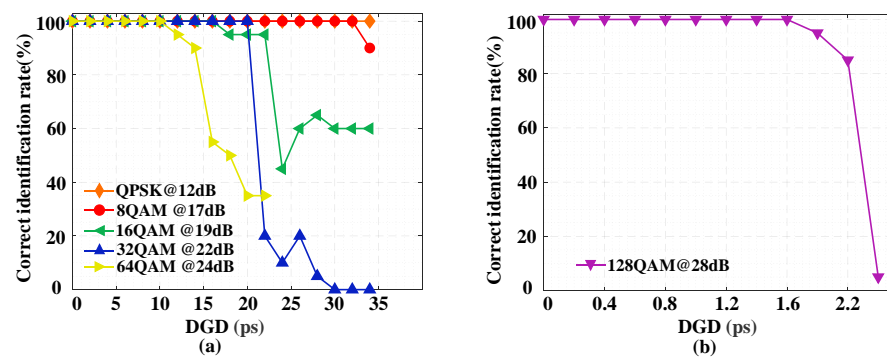


Figure 10. The tolerance with respect to the DGD for (a) QPSK, 8QAM, 16QAM, 32QAM, 64QAM and (b) 128QAM.

In order to analyze the effect of nonlinear impairments, a series of long-distance transmission simulations for QPSK (2000 km), 8QAM (1600 km), 16QAM (1040 km), 32QAM (400 km), 64QAM (160 km) and 128QAM (80 km) signals is conducted. The correct MFI rates of the six modulation formats versus the launch power in long-distance transmissions are shown in Figure 11. The proposed scheme can achieve 100% of the correct MFI rate even when the launch powers are increased to 10 dBm, 6 dBm, 4 dBm, 6 dBm, 4 dBm and 8 dBm for QPSK, 8QAM, 16QAM, 32QAM, 64QAM and 128QAM signals, respectively. These results demonstrate that the proposed MFI scheme is robust against fiber nonlinearities.

Finally, to comprehensively evaluate the performance of the proposed scheme with respect to other relevant MFI schemes based on deep neural network (DNN) [39] and SVM, their performance comparisons are made in Figure 12, where the number of symbols and histogram bins are fixed at 8000 and 40, respectively. The training sets for DNN and SVM comprise 9600 ($20 \times 80 \times 6$) amplitude histogram samples. For DNN, the numbers of neurons in the input, first hidden, second hidden and output layers are 40, 40, 10 and 6, respectively. The activation functions of the hidden layer and output layer are *ReLU* and *softmax*, respectively [40]. For SVM, the kernel function is the default radial basis function (RBF) kernel [41].

Based on the simulation results for both DNN and SVM, the minimum required OSNR comparisons between the proposed scheme and these two schemes based on DNN and SVM are shown in Figure 12. For QPSK, 8QAM, 16QAM, 32QAM and 64QAM, the minimum OSNR values required for achieving 100% of the correct MFI rate for the proposed scheme are lower than or equal to those corresponding to schemes based on DNN and SVM. Most importantly, only the proposed scheme can identify 128QAM over a wide OSNR range. Unlike the proposed scheme, the DNN and SVM just identify the global feature of the amplitude histogram. Since the characteristics of modulation formats are not effectively extracted based on the global feature of the amplitude histogram only, the MFI schemes based on DNN and SVM cannot identify 128QAM.

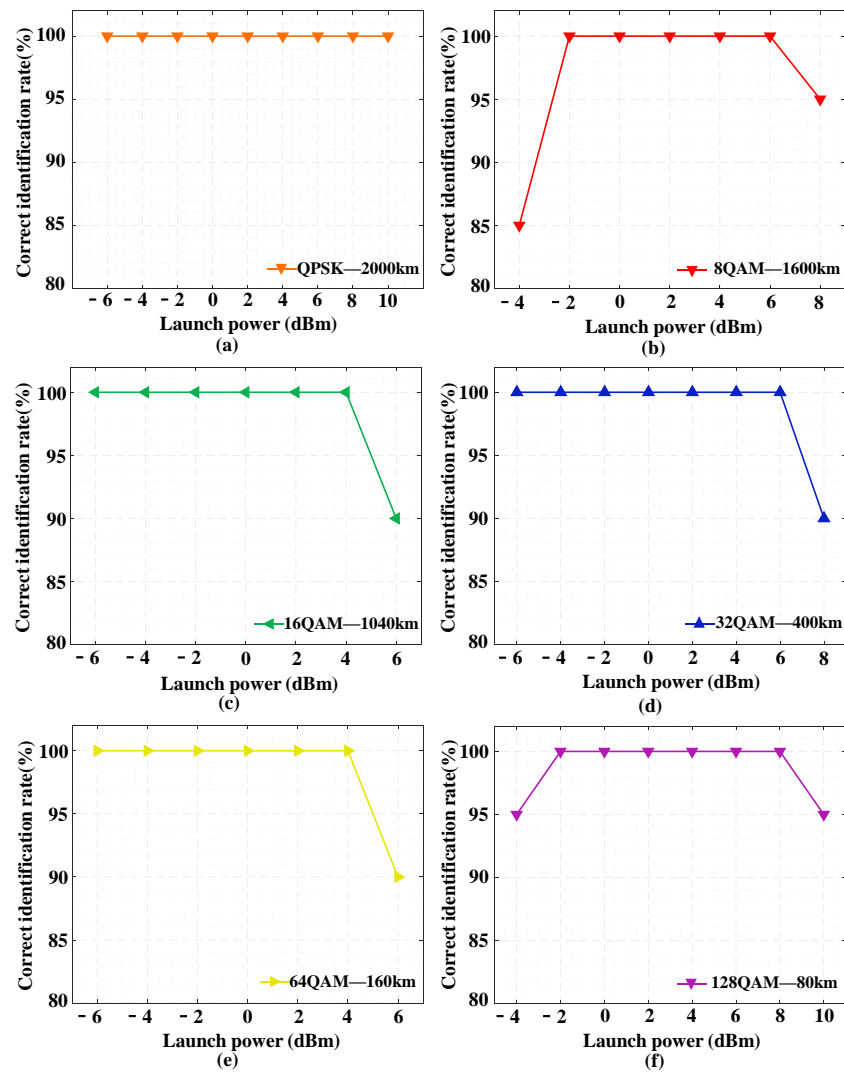


Figure 11. Correct MFI rates of the six modulation formats in the long-distance transmission. (a) QPSK, (b) 8QAM, (c) 16QAM, (d) 32QAM, (e) 64QAM, (f) 128QAM.

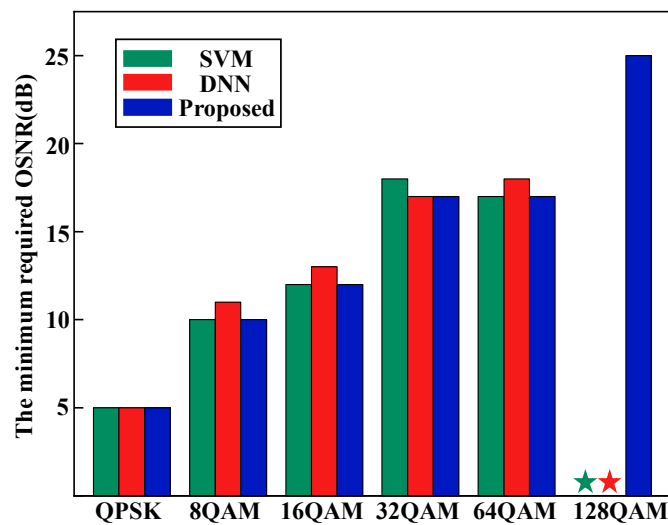


Figure 12. Minimum required OSNR for identifying different modulation formats for the three MFI schemes. The green and red star indicate that the modulation format is not identified by these two schemes.

To evaluate the computational complexity of the proposed scheme, the execution times for the three MFI schemes are analyzed. All of KNN, DNN and SVM are implemented by *MATLAB R2021a*, which run on a conventional computer equipped with a Core i7-10700 CPU at 2.9 GHz and 16 GB RAM. The graphics card is RTX2060 with 12 GB of memory. Unlike DNN and SVM, KNN does not require any training process. However, it should be noted that the training set for KNN needs to be introduced into *MATLAB R2021a*. The time of data input is 0.18 s, which is much less than the time used for the training of DNN and SVM, as shown in Figure 13a. Since the dimension of the extracted feature for the proposed scheme is only six, which is much less than the dimension of the amplitude histogram, the complexity of KNN is thus significantly reduced. The times used for the prediction of each testing sample in the three MFI schemes are depicted in Figure 13b. The time used for the prediction of the proposed scheme is also much less than those corresponding to the MFI schemes based on DNN and SVM. Therefore, the computational complexity of the proposed scheme is competitive.

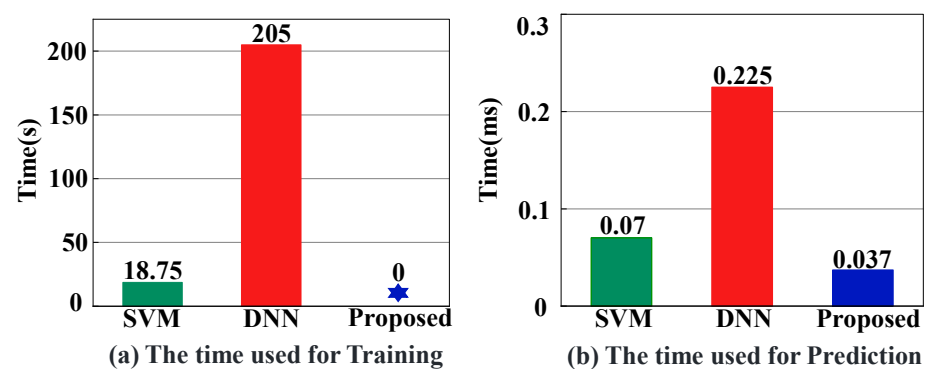


Figure 13. The execution times used for the (a) training process and (b) prediction process in the three MFI schemes. The blue star indicates that no training process is required for the proposed scheme.

4. Discussion

Although the selection of the six specific amplitude ranges is based on the characteristics of the considered modulation formats, it should be noted that no matter what the modulation format of an incoming signal is, all of the local features (N_1, N_2, N_3, N_4, N_5 and N_6) can be extracted, and the six specific amplitude ranges are fixed. The six-dimensional features of the incoming signals are constructed as an integrated whole.

On the one hand, as the order of the modulation format increases, the amplitude level may not be distinguishable, and thus, the effective feature extraction becomes much more difficult. On the other hand, the more modulation formats in the multi-dimensional space, the greater difficulty for distinguishing them is. Currently, the proposed scheme is not suitable for identifying modulation formats higher than 256QAM. This challenge will be addressed in our future work.

5. Conclusions

In this paper, a low-complexity MFI scheme based on multi-dimensional amplitude features has been proposed for digital coherent receivers in EONs. The proposed scheme has been verified based on numerical simulations with 28Gbaud PDM-QPSK/-8QAM/-16QAM/-32QAM/-64QAM/-128QAM signals. The results have shown that each modulation format can be identified with a 100% correct MFI rate when the OSNR values are greater than the corresponding theoretical 20% FEC limit. Meanwhile, the effects of the residual CD, PMD and fiber nonlinearities on the performance of the proposed scheme have also been discussed, and the results have shown that the proposed scheme is robust against both linear and nonlinear impairments. Furthermore, the computational complexity of the proposed scheme has been analyzed with appropriate comparisons being made with

relevant MFI schemes. The work indicates that the proposed scheme can be regarded as a good candidate for identifying modulation formats up to 128QAM.

Author Contributions: Conceptualization, M.H., W.H. and X.J.; methodology, M.H., W.H. and J.T.; software, M.H. and W.H.; validation, W.H. and S.L.; formal analysis, M.H., W.H. and J.T.; writing—original draft preparation, M.H. and W.H.; writing—review and editing, J.T., W.J. and L.C.; supervision, J.T.; project administration, M.H. and J.T.; funding acquisition, M.H. and J.T. All authors have read and agreed to the published version of the manuscript.

Funding: This research was partly supported by the Sichuan Science and Technology Program (2023YFH0067), partly supported by the European Regional Development Fund through Welsh Government, partly supported by the North Wales Growth Deal through Ambition North Wales, Welsh Government and UK Government and partly supported by the project of Sichuan University of Science and Engineering (2023RC23).

Institutional Review Board Statement: Not applicable.

Informed Consent Statement: Not applicable.

Data Availability Statement: Data underlying the results presented in this paper are not publicly available at this time but may be obtained from the authors upon reasonable request.

Acknowledgments: This work was supported by the program of China Scholarship Council (No. 202008515061).

Conflicts of Interest: The authors declare no conflicts of interest.

References

1. Ip, E.; Lau, A.P.T.; Barros, D.J.F.; Kahn, J.M. Coherent detection in optical fiber systems. *Opt. Express* **2008**, *16*, 753–791. [[CrossRef](#)] [[PubMed](#)]
2. Gerstel, O.; Jinno, M.; Lord, A.; Yoo, S.J.B. Elastic optical networking: A new dawn for the optical layer? *IEEE Commun. Mag.* **2012**, *50*, s12–s20. [[CrossRef](#)]
3. Hao, M.; Jiang, X.; Xiong, X.; Giddings, R.; He, W.; Tang, J. Low-complexity modulation format identification based on amplitude histogram distributions for digital coherent receivers. *Photonics* **2023**, *10*, 472. [[CrossRef](#)]
4. Jiang, X.; Hao, M.; Yan, L.; Jiang, L.; Xiong, X. Blind and low-complexity modulation format identification based on signal envelope flatness for autonomous digital coherent receivers. *Appl. Opt.* **2022**, *61*, 5991–5997. [[CrossRef](#)] [[PubMed](#)]
5. Yi, A.; Liu, H.; Yan, L.; Jiang, L.; Pan, Y.; Luo, B. Amplitude variance and 4th power transformation based modulation format identification for digital coherent receiver. *Opt. Commun.* **2019**, *452*, 109–115. [[CrossRef](#)]
6. Zhao, R.; Sun, W.; Xu, H.; Bai, C.; Tang, X.; Wang, Z.; Yang, L.; Cao, L.; Bi, Y.; Yu, X.; et al. Blind modulation format identification based on improved PSO clustering in a 2D Stokes plane. *Appl. Opt.* **2021**, *60*, 9933–9942. [[CrossRef](#)] [[PubMed](#)]
7. Eltaieb, R.A.; Abouelela, H.A.E.; Saif, W.S.; Ragheb, A.; Farghal, A.E.A.; Ahmed, H.E.H.; Alshebeili, S.; Shalaby, H.M.H.; El-Samie, F.E.A. Modulation format identification of optical signals: An approach based on singular value decomposition of Stokes space projections. *Appl. Opt.* **2020**, *59*, 5989–6004. [[CrossRef](#)] [[PubMed](#)]
8. Xiang, M.; Zhuge, Q.; Qiu, M.; Zhou, X.; Zhang, F.; Tang, M.; Liu, D.; Fu, S.; Plant, D.V. Modulation format identification aided hitless flexible coherent transceiver. *Opt. Express* **2016**, *24*, 15642–15655. [[CrossRef](#)] [[PubMed](#)]
9. Xiang, M.; Zhuge, Q.; Qiu, M.; Zhou, X.; Tang, M.; Liu, D.; Fu, S.; Plant, D.V. RF-pilot aided modulation format identification for hitless coherent transceiver. *Opt. Express* **2017**, *25*, 463–471. [[CrossRef](#)] [[PubMed](#)]
10. Fu, S.; Xu, Z.; Lu, J.; Jiang, H.; Wu, Q.; Hu, Z.; Tang, M.; Liu, D.; Chan, C.C. Modulation format identification enabled by the digital frequency-offset loading technique for hitless coherent transceiver. *Opt. Express* **2018**, *26*, 7288–7296. [[CrossRef](#)]
11. Borkowski, R.; Zibar, D.; Caballero, A.; Arlunno, V.; Monroy, I.T. Stokes space-based optical modulation format recognition for digital coherent receivers. *IEEE Photonics Technol. Lett.* **2013**, *25*, 2129–2132. [[CrossRef](#)]
12. Chen, P.; Liu, J.; Wu, X.; Zhong, K.; Mai, X. Subtraction-clustering-based modulation format identification in Stokes space. *IEEE Photonics Technol. Lett.* **2017**, *29*, 1439–1442. [[CrossRef](#)]
13. Mai, X.; Liu, J.; Wu, X.; Zhang, Q.; Guo, C.; Yang, Y.; Li, Z. Stokes space modulation format classification based on non-iterative clustering algorithm for coherent optical receivers. *Opt. Express* **2017**, *25*, 2038–2050. [[CrossRef](#)] [[PubMed](#)]
14. Hao, M.; Yan, L.; Yi, A.; Jiang, L.; Pan, Y.; Pan, W.; Luo, B. Stokes space modulation format identification for optical signals using probabilistic neural network. *IEEE Photonics J.* **2018**, *10*, 7202213. [[CrossRef](#)]
15. Yi, A.; Yan, L.; Liu, H.; Jiang, L.; Pan, Y.; Luo, B.; Pan, W. Modulation format identification and OSNR monitoring using density distributions in Stokes axes for digital coherent receivers. *Opt. Express* **2019**, *27*, 4471–4479. [[CrossRef](#)] [[PubMed](#)]
16. Cho, H.J.; Varughese, S.; Lippiatt, D.; Desalvo, R.; Tibuleac, S.; Ralph, S.E. Optical performance monitoring using digital coherent receivers and convolutional neural networks. *Opt. Express* **2020**, *28*, 32087–32104. [[CrossRef](#)] [[PubMed](#)]

17. Yu, X.; Bai, C.; Xu, H.; Sun, W.; Yang, L.; Zheng, H.; Hu, W. A modified PSO assisted blind modulation format identification scheme for elastic optical networks. *Opt. Commun.* **2020**, *476*, 126280. [[CrossRef](#)]
18. Wang, M.; Liu, J.; Zhang, J.; Zhang, D.; Guo, C. Modulation format identification based on phase statistics in Stokes space. *Opt. Commun.* **2021**, *480*, 126481. [[CrossRef](#)]
19. Xiang, Q.; Yang, Y.; Zhang, Q.; Yao, Y. Joint, accurate and robust optical signal-to-noise ratio and modulation format monitoring scheme using a single Stokes-parameter-based artificial neural network. *Opt. Express* **2021**, *29*, 7276–7287. [[CrossRef](#)] [[PubMed](#)]
20. Yu, X.; Bai, C.; Yang, L.; Xu, H.; Sun, W.; Li, J. Joint multi-parameter optical performance monitoring scheme based on trajectory information for a Stokes vector direct detection system. *Appl. Opt.* **2022**, *61*, 1606–1615. [[CrossRef](#)]
21. Guo, Z.; Liu, B.; Ren, J.; Wu, X.; Li, Y.; Mao, Y.; Chen, S.; Zhong, Q.; Zhu, X.; Wu, Y.; et al. Modulation format recognition with transfer learning assisted convolutional neural network using multiple Stokes sectional plane image in multi-core fibers. *Opt. Express* **2022**, *30*, 21990–22005. [[CrossRef](#)] [[PubMed](#)]
22. Jiang, L.; Yan, L.; Yi, A.; Pan, Y.; Bo, T.; Hao, M.; Pan, W.; Luo, B. Blind density-peak-based modulation format identification for elastic optical networks. *J. Lightwave Technol.* **2018**, *36*, 2850–2858. [[CrossRef](#)]
23. Bilal, S.M.; Bosco, G.; Dong, Z.; Lau, A.P.T.; Lu, C. Blind modulation format identification for digital coherent receivers. *Opt. Express* **2015**, *23*, 26769–26778. [[CrossRef](#)] [[PubMed](#)]
24. Liu, G.; Proietti, R.; Zhang, K.; Lu, H.; Yoo, S.B. Blind modulation format identification using nonlinear power transformation. *Opt. Express* **2017**, *25*, 30895–30904. [[CrossRef](#)] [[PubMed](#)]
25. Lin, X.; Eldemerdash, Y.; Dobre, O.; Zhang, S.; Li, C. Modulation classification using received signal's amplitude distribution for coherent receivers. *IEEE Photonics Technol. Lett.* **2017**, *29*, 1872–1875. [[CrossRef](#)]
26. Jiang, L.; Yan, L.; Yi, A.; Pan, Y.; Hao, M.; Pan, W.; Luo, B. An effective modulation format identification based on intensity profile features for digital coherent receivers. *J. Lightwave Technol.* **2019**, *37*, 5067–5075. [[CrossRef](#)]
27. Lu, J.; Tan, Z.; Lau, A.P.T.; Fu, S.; Tang, M.; Lu, C. Modulation format identification assisted by sparse-fast-Fourier-transform for hitless flexible coherent transceivers. *Opt. Express* **2019**, *27*, 7072–7086. [[CrossRef](#)] [[PubMed](#)]
28. Lv, H.; Zhou, X.; Huo, J.; Yuan, J. Joint OSNR monitoring and modulation format identification on signal amplitude histograms using convolutional neural network. *Opt. Fiber Technol.* **2021**, *61*, 102455. [[CrossRef](#)]
29. Zhang, Y.; Zhou, P.; Dong, C.; Lu, Y.; Li, C. Intelligent equally weighted multi-task learning for joint OSNR monitoring and modulation format identification. *Opt. Fiber Technol.* **2022**, *71*, 102931. [[CrossRef](#)]
30. Han, M.; Wang, M.; Fan, Y.; Cai, S.; Guo, Y.; Zhang, N.; Schatz, R.; Popov, S.; Ozolins, O.; Pang, X. Simultaneous modulation format identification and OSNR monitoring based on optoelectronic reservoir computing. *Opt. Express* **2022**, *30*, 47515–47527. [[CrossRef](#)]
31. Yang, F.; Bai, C.; Chi, X.; Zhang, R.; Qi, Q.; Sun, Z.; Xu, H.; Yang, L.; Bi, W.; Zhang, Y. Intelligent joint multi-parameter optical performance monitoring scheme based on HT images and MT-ResNet for elastic optical network. *Opt. Fiber Technol.* **2024**, *82*, 103599. [[CrossRef](#)]
32. Jiang, L.; Yan, L.; Yi, A.; Pan, Y.; Hao, M.; Pan, W.; Luo, B. Blind optical modulation format identification assisted by signal intensity fluctuation for autonomous digital coherent receivers. *Opt. Express* **2020**, *28*, 302–313. [[CrossRef](#)] [[PubMed](#)]
33. Feng, J.; Jiang, L.; Yan, L.; Yi, A.; Pan, W.; Luo, B. Intelligent Optical Performance Monitoring Based on Intensity and Differential-Phase Features for Digital Coherent Receivers. *J. Lightwave Technol.* **2022**, *40*, 3592–3601. [[CrossRef](#)]
34. Zhao, Z.; Yang, A.; Guo, P.; Tan, Q.; Xin, X. A modulation format identification method based signal amplitude sorting and ratio calculation. *Opt. Commun.* **2020**, *470*, 125819. [[CrossRef](#)]
35. Huang, Z.; Zhang, Q.; Xin, X.; Yao, H.; Gao, R.; Jiang, J.; Tian, F.; Liu, B.; Wang, F.; Tian, Q.; et al. Modulation format identification based on signal constellation diagrams and support vector machine. *Photonics* **2022**, *9*, 927. [[CrossRef](#)]
36. Ma, Y.; Gao, M.; Zhang, J.; Ye, Y.; Chen, W.; Ren, H.; Yan, Y. Modulation format identification based on constellation diagrams in adaptive optical OFDM systems. *Opt. Commun.* **2019**, *452*, 203–210. [[CrossRef](#)]
37. Zhang, Y.; Zhou, P.; Liu, Y.; Wang, J.; Li, C.; Lu, Y. Fast adaptation of multi-task meta-learning for optical performance monitoring. *Opt. Express* **2023**, *31*, 23183–23197. [[CrossRef](#)]
38. Kim, J.W.; Lee, C.H. Modulation format identification of square and non-square M-QAM signals based on amplitude variance and OSNR. *Opt. Commun.* **2020**, *474*, 126084. [[CrossRef](#)]
39. Khan, F.N.; Zhong, K.; Al-Arashi, W.H.; Yu, C.; Lu, C.; Lau, A.P.T. Modulation Format Identification in Coherent Receivers Using Deep Machine Learning. *IEEE Photonics Technol. Lett.* **2016**, *28*, 1886–1889. [[CrossRef](#)]
40. Zhao, Y.; Shi, C.; Wang, D.; Chen, X.; Wang, L.; Yang, T.; Du, J. Low-Complexity and Nonlinearity-Tolerant Modulation Format Identification Using Random Forest. *IEEE Photonics Technol. Lett.* **2019**, *31*, 853–856. [[CrossRef](#)]
41. Lin, X.; Dobre, O.A.; Ngatched, T.M.N.; Eldemerdash, Y.A.; Li, C. Joint Modulation Classification and OSNR Estimation Enabled by Support Vector Machine. *IEEE Photonics Technol. Lett.* **2018**, *30*, 2127–2130. [[CrossRef](#)]

Disclaimer/Publisher's Note: The statements, opinions and data contained in all publications are solely those of the individual author(s) and contributor(s) and not of MDPI and/or the editor(s). MDPI and/or the editor(s) disclaim responsibility for any injury to people or property resulting from any ideas, methods, instructions or products referred to in the content.